Forming a Double-Helix Phase of Single Polymer Chains by the Cooperation between Local Structure and Nonlocal Attraction

Jiang Du,[1,*] Hongmei Yin,[1,*] Haoqi Zhu,[2,*] Tiantian Wan,[1] Binzhou Wang,[1] Hongtao Qi,[1] Yanfang Lu,[1]
Liang Dai,[2,†] and Tao Chen[1,‡]
[1]*College of Chemistry and Materials Science, Northwest University, Xi'an 710127, China*
[2]*Department of Physics, City University of Hong Kong, Hong Kong 999077, China*

(Received 11 November 2021; revised 1 March 2022; accepted 25 March 2022; published 9 May 2022)

Double-helix structures, such as DNA, are formed in nature to realize many unique functions. Inspired by this, researchers are pursuing strategies to design such structures from polymers. A key question is whether the double helix can be formed from the self-folding of a single polymer chain without specific interactions. Here, using Langevin dynamics simulation and theoretical analysis, we find that a stable double-helix phase can be achieved by the self-folding of single semiflexible polymers as a result of the cooperation between local structure and nonlocal attraction. The critical temperature of double-helix formation approximately follows $T^{\mathrm{cri}} \sim \ln(k_\theta)$ and $T^{\mathrm{cri}} \sim \ln(k_\tau)$, where k_θ and k_τ are the polymer bending and torsion stiffness, respectively. Furthermore, the double helix can exhibit major and minor grooves due to symmetric break for better packing. Our results provide a novel guide to the experimental design of the double helix.

DOI: 10.1103/PhysRevLett.128.197801

Double-helix structures are widely observed in nature and exert many unique biological functions, such as information storage and replication [1]. Inspired by this, researchers are working on designing double helices to host versatile functions, including molecular recognition and asymmetric catalysis [2–4]. To date, the strategies determined to construct double-helix structures are mainly based on hydrogen bonding, π-π interactions, or metal coordination [3–7], which rely on specific interactions of chemical structures [8,9]. Despite these advances, the design of the double-helix structures remains challenging, particularly, the nature of the chain elements of the polymers that exhibit the double-helix structures is still elusive.

From the physical viewpoint, a key question is what is the minimal polymer model that can reach a double helix by self-folding, without resorting to complicated and special chemical structures and interactions. Many efforts have been made to explore structures and phase transitions of single flexible or semiflexible polymer chains [10–25], however, the double-helix structures have never been observed. Nonspecific intermonomer attractions usually lead to globular structures rather than double helix, because globular structures can maximize the number of attractive pairs. To suppress the formation of globular structures and promote the formation of a double helix, bending stiffness k_θ and torsion stiffness k_τ can be introduced into the polymer model. Considering that a double helix has rather uniform bending and torsion, adding intrinsic bond angle θ_0 and intrinsic torsion angle τ_0 can further strengthen the tendency of a polymer to fold into a double helix. Here, θ_0 and τ_0 correspond to the situation with zero bending and torsion energy. In principle, in the case of $k_\theta = +\infty$ and $k_\tau = +\infty$, a polymer chain can fold into a single helix with geometrical features specified by θ_0 and τ_0. However, $k_\theta = +\infty$ and $k_\tau = +\infty$ are usually unrealistic for real polymers. We are more interested in the regime where k_θ and k_τ are moderate and the double-helix structures compete with the globular structures in terms of free energy. In such a regime, it is difficult to estimate from theory whether double-helix or globular structures are thermodynamically more stable. In this Letter, we will employ a highly efficient sampling method to investigate the phase diagram of double-helix or globular structures for a generic polymer model with moderate k_θ and k_τ.

Here, a generic coarse-grained bead-spring model, containing bending, torsion, and self-attraction potentials, is employed. Considering that the formation of a sharp turn in the double helix will produce a considerable energetic penalty, the two middle beads along the semiflexible homopolymer chain are replaced by the two flexible ones, namely $B_nL_2B_n$, in which the B_n is a semiflexible strand composed of n beads of B and the L_2 represents two flexible beads of L. Then the chain length N is $2n+2$. The bonded beads along the chain interact via a harmonic potential E_{bon}, described as $E_{\mathrm{bon}} = \sum_i k_r \varepsilon (r_i - \sigma)^2$, where $k_r = 100$ is a stiff spring constant [23], $\varepsilon = 1$ is the energy scale, r_i is the length of bond connecting successive beads, and $\sigma = 4$ is the length scale. To simulate chain stiffness, the bending potential E_{ben} for the B_n strands is given by $E_{\mathrm{ben}} = \sum_i k_\theta \varepsilon (\theta_i - \theta_0)^2$, where θ_i is the angle between two adjacent bonds formed by B beads at any given configuration, and θ_0 corresponds to the equilibrium bond angle [19,23]. The torsion potential $E_{\rm tor}$ for the B_n strands is given by $E_{\rm tor} = \sum_i k_\tau \varepsilon[1 - \cos(\tau_i - \tau_0)]$, where τ_i is the torsion angle, and τ_0 is its equilibrium value [24,25]. The effective nonbonded pairwise attractive interactions $E_{\rm con}$ between B beads in dilute solution are described by the form of Lennard-Jones (LJ) potential $E_{\rm con} = \sum \varepsilon[(\sigma/r_{ij})^{12} - 2(\sigma/r_{ij})^6]$, in which r_{ij} is the distance between two beads i and j [20,26]. In order to improve the computational efficiency, a common cutoff value $r_c = 2.5\sigma$ is included, at which the LJ potential approximates to -0.008ε, that is, if $r_{ij} > r_c$, the LJ potential is zero. The nonbonded potential between L and B is purely repulsive, given by $E_{\rm rep} = \sum \varepsilon(\sigma/r_{ij})^{12}$. Accordingly, the potential energy is expressed by $E_p = E_{\rm bon} + E_{\rm ben} + E_{\rm tor} + E_{\rm con} + E_{\rm rep}$. In the following study, the values of reference angles θ_0 and τ_0 are set to 1.832 and 0.873, respectively, corresponding to 105° and 50°, unless otherwise specified. The choice, derived from the prediction by a theoretical method in the Supplemental Material [27], allows for the formation of a double-helix structure. In simulations, Langevin dynamics in combination with replica-exchange method (REM) sampling is performed [23,36].

Figures 1(a) and 1(b) present the structural pseudophase diagrams [37] for the polymers of length $N = 30$. With the variations of k_θ, k_τ, and T, polymer conformations can transition among distinct structures as illustrated in Figs. 1(a)–1(c). See the detailed analysis of the transitions in Secs. S1–S4 [27]. One feature of the phase diagrams is that the double-helix structures (DH_1) can be formed only at sufficiently large k_θ and k_τ. The minimum parameter sets of (k_θ, k_τ) for DH_1 formation is presented in Fig. 1(d).

The formation of DH_1 usually causes the entropy loss, which is compensated by lowering the bending and torsion energy and enhancing interstrand attractions. Accordingly, DH_1 formation often occurs at sufficiently low temperature. We calculate the entropy loss, ΔS, for the $G^* - DH_1$ transition and find that $|\Delta S|$ is smaller with the decrease of k_θ and k_τ [Fig. 1(e)]. The minimal $|\Delta S|$ is ~12.5 or 0.42 per bead. To ascertain the free energy barrier to form DH_1, a free energy landscape is shown in Fig. 1(f).

Next, we perform a theoretical analysis of the $G^* - DH_1$ transition using an approach similar to the thermodynamic integration. Only key steps are presented here, and more details can be found in Sec. S7 [27]. Polymer conformational free energy is defined as $F = -k_B T \ln \Sigma_j \exp(-E_j/k_B T)$, where E_j is the total energy of conformation j. The dependence of F on k_θ can be expressed as

$$\partial F/\partial k_\theta = \langle \partial E_p/\partial k_\theta \rangle. \qquad (1)$$

Here, $\langle\rangle$ refers to the ensemble average. For our polymer model, $\partial E_p/\partial k_\theta$ is determined as

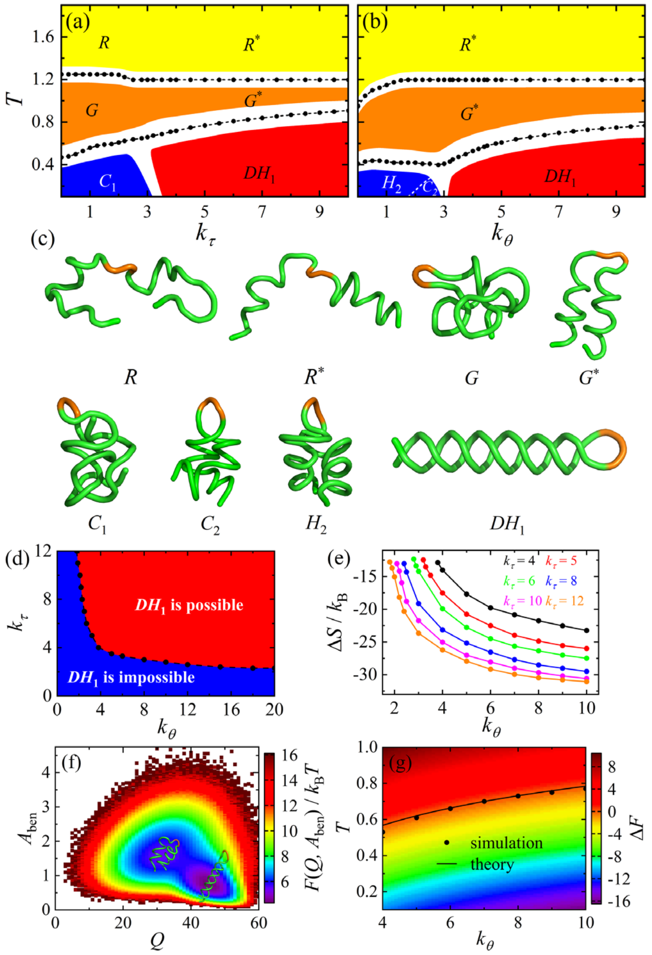

FIG. 1. Phase diagrams for the self-folding of single semiflexible polymers of length $N = 30$ with reference angles $\theta_0 = 105°$ and $\tau_0 = 50°$. (a) Varying the torsion stiffness k_τ and the temperature T at a fixed bending stiffness $k_\theta = 10$. (b) Varying k_θ and T at $k_\tau = 5$. The dotted lines represent the transition temperatures. Colored regions stand for structural phases. (c) Representative structures in different phases: random coils (R), random coils with flickering helical ordering (R^*), globules (G), globules with local helical ordering (G^*), compact structures (C_1), compact structures with local helical ordering (C_2), two-helix bundles (H_2), and double-helix structures (DH_1). The linker in the polymer is marked in orange. (d) The minimum parameter sets of k_θ and k_τ for the formation of DH_1. (e) The dependence of entropy loss, ΔS, for the $G^* - DH_1$ transition on k_θ and k_τ at their respective transition temperatures. (f) The free energy landscape for the $G^* - DH_1$ equilibrium at $k_\theta = 7$, $k_\tau = 5$, and $T = 0.7$. (g) The free energy difference $\Delta F = F_{DH_1} - F_{G^*}$ at $k_\tau = 5$. The transition temperatures corresponding to $\Delta F = 0$ are obtained from simulations and Eq. (9).

$$\partial E_p/\partial k_\theta = \partial E_{\rm ben}/\partial k_\theta = \Sigma_i(\theta_i - \theta_0)^2 \equiv A_{\rm ben}. \qquad (2)$$

Here, $A_{\rm ben}$ characterizes the total curvature of a conformation. Combining Eqs. (1) and (2), we obtain the free energy change upon k_θ variation:

$$F(k_\theta^b) - F(k_\theta^a) = \int_{k_\theta^a}^{k_\theta^b} \langle A_{\mathrm{ben}} \rangle dk_\theta. \qquad (3)$$

Then, we apply Eq. (3) to the $G^* - DH_1$ transition. We define the free energy difference between DH_1 and G^* phases as ΔF, which can be derived through

$$\Delta F \equiv F_{DH_1}(k_\theta) - F_{G^*}(k_\theta) = \int_{k_\theta^{\mathrm{ref}}}^{k_\theta} \Delta A_{\mathrm{ben}} dk_\theta,$$
$$\text{with} \quad \Delta A_{\mathrm{ben}} \equiv \langle A_{\mathrm{ben}}^{DH_1} \rangle - \langle A_{\mathrm{ben}}^{G^*} \rangle. \qquad (4)$$

The integration starts at k_θ^{ref}, which corresponds to the $G^* - DH_1$ equilibrium, i.e., $F_{DH_1}(k_\theta^{\mathrm{ref}}) - F_{G^*}(k_\theta^{\mathrm{ref}}) = 0$. Equation (4) has a clear physical meaning that the difference in the curvatures between DH_1 and G^* conformations is responsible for the dependence of ΔF on k_θ. Our simulations suggest that $\Delta A_{\mathrm{ben}} \approx \Delta E_{\mathrm{ben}}/k_\theta$, while ΔE_{ben} is nearly a constant over a wide range of k_θ. Taking advantage of this, we obtain

$$\Delta F \approx \Delta E_{\mathrm{ben}} \ln(k_\theta / k_\theta^{\mathrm{ref}}). \qquad (5)$$

Using similar approaches, we obtain the free energy change upon varying k_τ around the $G^* - DH_1$ equilibrium:

$$\Delta F \approx \Delta E_{\mathrm{tor}} \ln(k_\tau / k_\tau^{\mathrm{ref}}). \qquad (6)$$

Similarly, free energy change caused by varying T around the $G^* - DH_1$ equilibrium follows

$$\Delta F \approx -(T - T^{\mathrm{ref}})\Delta S, \qquad (7)$$

where $\Delta S \equiv S_{DH_1} - S_{G^*}$ is the difference in entropy between the two phases. Combining Eqs. (5)–(7) leads to

$$\Delta F \approx \Delta E_{\mathrm{ben}} \ln\left(\frac{k_\theta}{k_\theta^{\mathrm{ref}}}\right) + \Delta E_{\mathrm{tor}} \ln\left(\frac{k_\tau}{k_\tau^{\mathrm{ref}}}\right) - (T - T^{\mathrm{ref}})\Delta S. \qquad (8)$$

Equation (8) can be used to calculate the stability of DH_1 with respect to G^* as a function of k_θ, k_τ, and T. Here, $(k_\theta^{\mathrm{ref}}, k_\tau^{\mathrm{ref}}, T^{\mathrm{ref}})$ is a parameter set at the $G^* - DH_1$ equilibrium. Figure 1(g) presents a 2D plot of ΔF for $k_\theta^{\mathrm{ref}} = 7$, $k_\tau^{\mathrm{ref}} = 5$, and $T^{\mathrm{ref}} = 0.7$. For this parameter set, we obtain $\Delta E_{\mathrm{ben}} = -5.66$, $\Delta E_{\mathrm{tor}} = -4.86$, and $\Delta S = -23.98$.

Equation (8) can be also used to derive the dependence of the $G^* - DH_1$ transition temperature T^{cri} on k_θ. For a fixed k_τ, the $G^* - DH_1$ equilibrium corresponds to $\Delta F = 0$, i.e., $\Delta E_{\mathrm{ben}} \ln(k_\theta / k_\theta^{\mathrm{ref}}) - (T^{\mathrm{cri}} - T^{\mathrm{ref}})\Delta S \approx 0$, which yields

$$T^{\mathrm{cri}} \approx T^{\mathrm{ref}} + (\Delta E_{\mathrm{ben}}/\Delta S) \ln(k_\theta / k_\theta^{\mathrm{ref}}). \qquad (9)$$

As shown by the solid line in Fig. 1(g), the prediction of Eq. (9) agrees with the phase boundary obtained from simulations. More comparisons between theory and simulation are included in Sec. S7 [27].

We find that double helix is most favorable when the local polymer structure, which is largely determined by θ_0 and τ_0, can maximize the contact area between two strands. To elaborate this idea, we carried out the following analysis. For each set of θ_0 and τ_0, we define an ideal double helix with $\theta = \theta_0$ and $\tau = \tau_0$, i.e., $E_{\mathrm{ben}} = 0$ and $E_{\mathrm{tor}} = 0$. In the structure, the relative position between two helices is set to optimize the attractive energy, defined as $E_p(\theta_0, \tau_0)$. Herein, if $E_p(\theta_0, \tau_0)/N \leq -0.5$, the double helix is expected to emerge. Otherwise, it could not form because the gaps in one helix are too small to accommodate the other. In principle, the value of $E_p(\theta_0, \tau_0)/N$ is associated with the contact area between the two helices, and the larger the contact area is, the lower the $E_p(\theta_0, \tau_0)/N$ becomes. As displayed in Fig. 2(a), the formation of double-helix structures depends on both θ_0 and τ_0, and within the ranges $\theta_0 < 93°$ or $\tau_0 > 85°$ it is difficult to adopt a double-helix conformation due to $E_p(\theta_0, \tau_0)/N > -0.5$. In the region of $100° < \theta_0 < 110°$ and $50° \leq \tau_0 \leq 60°$, the contact area between the two helices should be larger than that in the other regions due to $E_p(\theta_0, \tau_0)/N < -2.2$ [Fig. 2(a)]. We noted that the ideal DH_1 structures are present within the ranges $42° \leq \tau_0 \leq 78°$ for $\theta_0 = 105°$ and $97° \leq \theta_0 \leq 159°$ for $\tau_0 = 50°$.

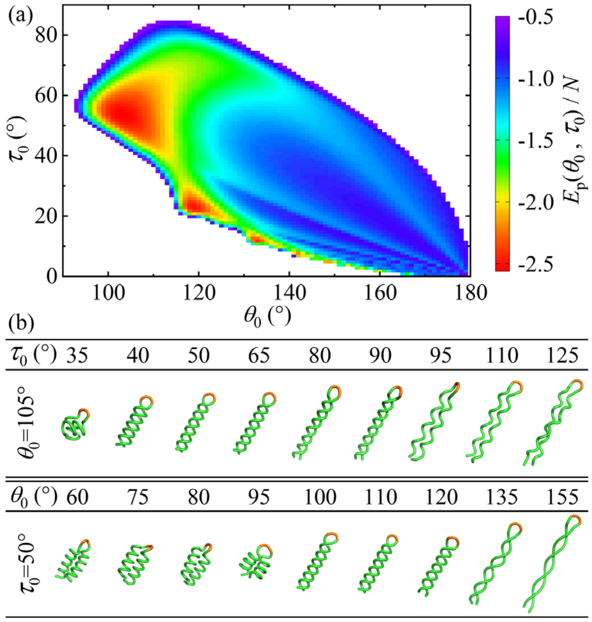

FIG. 2. Influence of local structure on the formation of double helix. (a) The energy per bead $E_p(\theta_0, \tau_0)/N$ of the ideal double-helix structures, constructed by the theoretical method, as functions of θ_0 and τ_0. Note that the region for $E_p(\theta_0, \tau_0)/N > -0.5$, where the gaps in one helix cannot accommodate the other, is marked in white. (b) Typical simulated structures for a variety of values of θ_0 and τ_0 for the 30mer with $k_\theta = 10$ and $k_\tau = 10$ at $T = 0.1$.

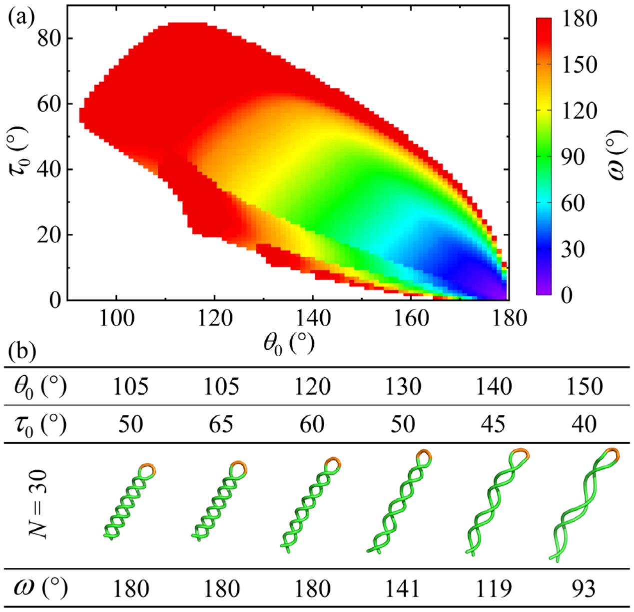

θ_0 (°)	105	105	120	130	140	150
τ_0 (°)	50	65	60	50	45	40
ω (°)	180	180	180	141	119	93

FIG. 3. Local structure effect on the formation of major and minor grooves in the double-helix structures. (a) The dependence of the theoretical azimuthal angle ω between two helical strands on θ_0 and τ_0. (b) The representative simulated structures of the 30mer with $k_\theta = 10$ and $k_\tau = 10$ for a number of values of θ_0 and τ_0 at $T = 0.1$, and the corresponding simulated values of ω shown at the bottom.

This prediction is supported by the simulations [Fig. 2(b)]. For the polymers of $N = 30$ with $\theta_0 = 105°$, within the range $40° \leq \tau_0 \leq 90°$ the representative simulated structures are double helix at low temperatures. However, for $\tau_0 \leq 35°$ or $\tau_0 \geq 95°$ the typical structures are amorphous or hairpinlike, respectively. Although the simulated double-helix structures occur at $\tau_0 = 90°$, the average torsion angles of these conformations approximate to 76°, deviated from the given reference angle, because the local constraints in the simulations are not as strong as those in the theoretical method. As the τ_0 is fixed at 50°, the representative structures are two-helix bundles for $60° \leq \theta_0 \leq 95°$, but double helix for $100° \leq \theta_0 \leq 155°$, consistent with the theoretical prediction. Interestingly, for $\theta_0 = 100°$ and $\tau_0 = 50°$, it was reported that the homopolymer exhibits the helix bundles at low temperature [24,25]. However, the double-helix structures are present in our study. One possible reason is the effect of the attractive potential range. In that work, the attractive potential function is given by $v_{LJ} = 4\varepsilon[(\sigma/r_{ij})^{12} - (\sigma/r_{ij})^6]$, differing from that in our model (Fig. S11a [27]). By adopting the v_{LJ} potential, the region in terms of θ_0 and τ_0, expected to form the double helix, is determined by the theoretical method (Fig. S11b [27]). Intriguingly, this region falls within that predicted by our model [Fig. 2(a)], but does not include $\theta_0 = 100°$ and $\tau_0 = 50°$, namely, at these reference angles the gaps in one helix cannot accommodate the other. This result indicates that the interaction range between chain elements affects the formation of the double helix.

The major and minor grooves often occur in some double-helix structures of DNA as a consequence of the asymmetry of complementary base pairs [38]. Are the major and minor grooves present in the double-helix structures formed from homopolymers lacking such asymmetry? For this purpose, the influence of the local structure of the polymers on the formation of the major and minor grooves has been examined.

The ideal double helices for various values of θ_0 and τ_0 within the ranges, where the DH_1 conformations are expected to emerge [Fig. 2(a)], are constructed by the theoretical method [27]. To identify major and minor grooves, the azimuthal angle ω, defined as the angle by which one helical strand rotates to coincide with the other around the axis of the double helix, is employed. If $\omega < 180°$, the major and minor grooves are present. As shown in Fig. 3(a), the regions of reference angles in favor of forming major and minor grooves are surrounded by those apt to adopting the symmetric double-helix structures, and generally, the polymers with larger θ_0 and smaller τ_0 tend to adopt the double-helix conformations containing major and minor grooves. To confirm the prediction, the simulations are performed for the 30mer with $k_\theta = 10$ and $k_\tau = 10$ for a number of pairs of θ_0 and τ_0 [Fig. 3(b) and video S1 in Ref. [27]]. Indeed, the azimuthal angles of the simulated double helices are in good agreement with the angles obtained from the theoretical analysis. To understand how the local structure affects the formation of the major and minor grooves, the helical pitch (h) and the diameter (d) of a single helix, depending on the values of θ_0 and τ_0, have been calculated (Fig. S12 [27]). When the value of $d - \sigma$ approaches to σ or the value of h is close to 2σ, the two helices are able to get sufficient contact in the direction perpendicular or parallel to the axis of the double helix, favoring pairwise attraction, and leading to the formation of the symmetric double helix. However, when the values of d and h are large enough, the two helices almost could not get contact for a symmetric double helix, and in this case, although entropically favorable, it is energetically unfavorable. Therefore, at low temperature, to optimize pairwise attractions, the two helices need to rotate by a certain angle around the axis of the double helix to gain adequate contact, causing symmetric break and the occurrence of the major and minor grooves.

For finite systems, the system size should have a significant impact on the structural geometry and stability. To get insight into the chain-length effect on the formation of double-helix structures, the diagram of states in terms of k_τ and T for the 50mer with $\theta_0 = 105°$, $\tau_0 = 50°$, and $k_\theta = 10$ is plotted (Fig. 4). Compared to the diagram of states for $N = 30$, the phase diagram for $N = 50$ exhibits apparently more structures in the folded regime. For low temperatures, within the range $0 \leq k_\tau \leq 1.0$ the self-attractions overcome bending and torsion constraints,

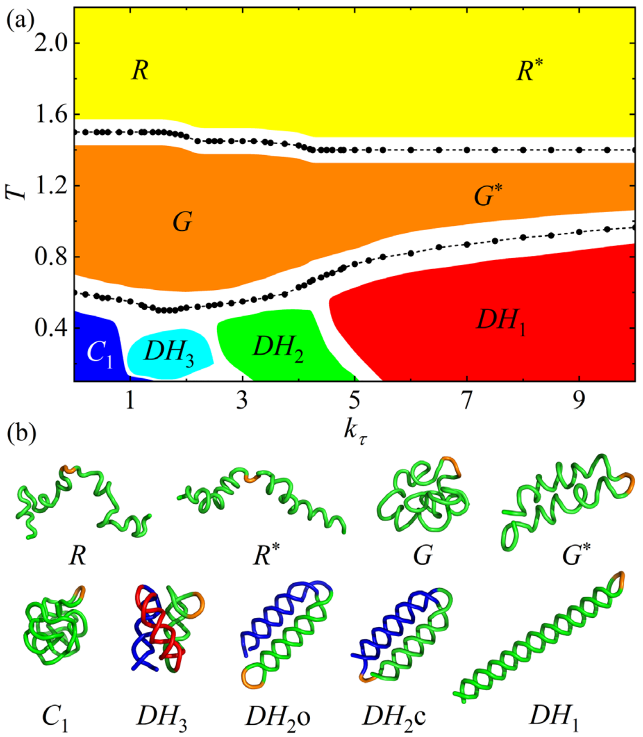

FIG. 4. (a) Phase diagram in terms of k_τ and T for the semiflexible polymers of $N = 50$ with $\theta_0 = 105°$, $\tau_0 = 50°$ and $k_\theta = 10$. The transition temperatures corresponding to the coil-globule or freezing transition are depicted by the black symbols connected by the dotted lines. (b) Typical structures as marked in the phase diagram. They are composed of R, R^*, G, G^*, and C_1, three-double-helix bundles (DH_3), opened two-double-helix bundles (DH_2o), closed two-double-helix bundles (DH_2c), and DH_1 structures.

and the compact amorphous structures (C_1) predominate. With the increase of k_τ, the three-double-helix bundles (DH_3) occur for $1.0 < k_\tau < 2.4$, and the two-double-helix bundles (DH_2) emerge for $2.6 < k_\tau < 5.0$. Upon further increasing k_τ, a stable double-helix phase (DH_1) is present for $k_\tau > 5.5$. Obviously, the torsion strength required to stabilize the DH_1 structure for the 50mer is larger than that for the 30mer [Figs. 1(a) and 4(a)], which should be attributed to the fact that as the chain length increases, the possible pairwise attractions increase, leading to the enhancement of the torsion strength to preserve the double-helix structure. With further increasing the chain length, additional structures are observed. See more discussion about the chain-length dependence in Secs. S8 and S10 [27].

The above simulations do not consider Coulomb interactions within the polymer chains. We have performed additional simulations with Coulomb interactions and also observed double helix (Sec. S11) [27].

In conclusion, we obtain the parameter spaces $(k_\theta, k_\tau, \theta_0, \tau_0, T, N)$ for the double-helix formation in the self-folding of a generic polymer model. More importantly, we reveal the physical roles of each parameter in double-helix formation. First, the entropy loss in the double-helix formation must be compensated by lowering the bending and torsion energies, which requires k_θ and k_τ to be sufficiently large [Fig. 1(d)]. Second, the shape of local structures determined by θ_0 and τ_0 should facilitate the interhelix contacts to enhance pairwise attractions (Fig. 2). Third, the major and minor grooves can be controlled by θ_0 and τ_0. Fourth, increasing N promotes the formation of the double-helix bundles, which can be suppressed by higher k_θ and k_τ. The proper combination of θ_0, τ_0, k_θ, and k_τ should play important roles in the double-helix formation in experiments of synthetic semiflexible polymers [7,39,40]. In addition, a series of very interesting experiments observed that polyalanines exhibit several distinct conformations including globule, single helix, and helical dimer (bundle), depending on the chain length and the addition of lysine on the C- or N- terminus [41,42]. Double helix is absent in polyalanines probably because θ_0, τ_0, k_θ, and k_τ are not in the region. Interestingly, the equilibrium angles of the helix formed by the polyalanines are $\theta_0 \approx 91°$ and $\tau_0 \approx 50°$, which are not within the DH_1 region (Fig. S27b [27]), but rather within α-helix region (Fig. S27c [27]). Accordingly, our results are useful in choosing θ_0, τ_0, k_θ, and k_τ for rational design of the double helix in real polymers.

This work was supported by the National Natural Science Foundation of China (No. 21875187 and No. 21973080).

---

[*] These authors contributed equally to this work.

[†] Corresponding author.
liangdai@cityu.edu.hk

[‡] Corresponding author.
tchen@nwu.edu.cn

[1] J. D. Watson and F. H. C. Crick, Nature (London) **171**, 964 (1953); **171**, 737 (1953).
[2] T. Hasegawa, Y. Furusho, H. Katagiri, and E. Yashima, Angew. Chem. Int. Ed. **46**, 5885 (2007).
[3] J. Liu, Z. Luo, L. Yu, P. Zhang, H. Wei, and Y. Yu, Chem. Sci. **11**, 8224 (2020).
[4] E. Yashima, K. Maeda, and Y. Furusho, Acc. Chem. Res. **41**, 1166 (2008).
[5] E. Yashima, N. Ousaka, D. Taura, K. Shimomura, T. Ikai, and K. Maeda, Chem. Rev. **116**, 13752 (2016).
[6] Y. Hu, S. J. Teat, W. Gong, Z. Zhou, Y. Jin, H. Chen, J. Wu, Y. Cui, T. Jiang, X. Cheng, and W. Zhang, Nat. Chem. **13**, 660 (2021).
[7] Y. Wang *et al.*, Nat. Commun. **10**, 801 (2019).
[8] R. Frederickx, T. in't Veld, and E. Carlon, Phys. Rev. Lett. **112**, 198102 (2014).
[9] H. Li and A. Kabakçıoğlu, Phys. Rev. Lett. **121**, 138101 (2018).
[10] P. G. de Gennes, *Scaling Concepts in Polymer Physics* (Cornell University Press, Ithaca, 1979).
[11] Y. Zhou, C. K. Hall, and M. Karplus, Phys. Rev. Lett. **77**, 2822 (1996).

[12] F. Rampf, W. Paul, and K. Binder, Europhys. Lett. **70**, 628 (2005).

[13] S. Schnabel, T. Vogel, M. Bachmann, and W. Janke, Chem. Phys. Lett. **476**, 201 (2009).

[14] R. Wang and Z.-G. Wang, Macromolecules **47**, 4094 (2014).

[15] Q. Wei, R. G. Melko, and J. Z. Y. Chen, Phys. Rev. E **95**, 032504 (2017).

[16] M. R. Stukan, V. A. Ivanov, A. Yu. Grosberg, W. Paul, and K. Binder, J. Chem. Phys. **118**, 3392 (2003).

[17] B. Schnurr, F. C. MacKintosh, and D. R. M. Williams, Europhys. Lett. **51**, 279 (2000).

[18] A. Montesi, M. Pasquali, and F. C. MacKintosh, Phys. Rev. E **69**, 021916 (2004).

[19] Z. Ou and M. Muthukumar, J. Chem. Phys. **123**, 074905 (2005).

[20] D. T. Seaton, S. Schnabel, D. P. Landau, and M. Bachmann, Phys. Rev. Lett. **110**, 028103 (2013).

[21] T. X. Hoang, A. Giacometti, R. Podgornik, N. T. T. Nguyen, J. R. Banavar, and A. Maritan, J. Chem. Phys. **140**, 064902 (2014).

[22] M. Marenz and W. Janke, Phys. Rev. Lett. **116**, 128301 (2016).

[23] J. Wu, C. Cheng, G. Liu, P. Zhang, and T. Chen, J. Chem. Phys. **148**, 184901 (2018).

[24] M. J. Williams and M. Bachmann, Phys. Rev. Lett. **115**, 048301 (2015).

[25] M. J. Williams and M. Bachmann, Phys. Rev. E **93**, 062501 (2016).

[26] E. P. O'Brien, G. Ziv, G. Haran, B. R. Brooks, and D. Thirumalai, Proc. Natl. Acad. Sci. U.S.A. **105**, 13403 (2008).

[27] See Supplemental Material at http://link.aps.org/supplemental/10.1103/PhysRevLett.128.197801 for identification of structural phases, analysis of the order of phase transitions and the structures of H_2 and DH_1, the detailed analysis of phase diagrams, simulation results of the energy changes during the double-helix formation, comparison of our simulations and the simulations by Williams *et al.*, construction of ideal double-helix structures by a theoretical method, theoretical derivation of free energy changes using the thermodynamic integration, chain-length dependence and long-chain limit of the transition temperature of double helix, energy and entropy changes of the $DH_1 - DH_2$ transition, typical structures of longer polymer chains and polypeptides, effect of Coulomb interactions on the double-helix formation, and snapshots of the double-helix structures with major and minor grooves, which includes Refs. [28–35].

[28] P. Palenčár and T. Bleha, Comput. Theor. Chem. **1006**, 62 (2013).

[29] P. Palenčár and T. Bleha, J. Chem. Phys. **141**, 174901 (2014).

[30] L. W. Zilch, D. T. Kaleta, M. Kohtani, R. Krishnan, and M. F. Jarrold, J. Am. Soc. Mass Spectrom. **18**, 1239 (2007).

[31] M. F. Jarrold, Phys. Chem. Chem. Phys. **9**, 1659 (2007).

[32] M. Kohtani, J. E. Schneider, T. C. Jones, and M. F. Jarrold, J. Am. Chem. Soc. **126**, 16981 (2004).

[33] F. O. Tzul, K. L. Schweiker, and G. I. Makhatadze, Proc. Natl. Acad. Sci. U.S.A. **112**, E259 (2015).

[34] R. Owczarzy, Y. You, B. G. Moreira, J. A. Manthey, L. Huang, M. A. Behlke, and J. A. Walder, Biochemistry **43**, 3537 (2004).

[35] K. Rippe, N. B. Ramsing, and T. M. Jovin, Biochemistry **28**, 9536 (1989).

[36] A. Mitsutake, Y. Sugita, and Y. Okamoto, Biopolymers **60**, 96 (2001).

[37] At such mesoscopic scales, prevalent in biologically relevant systems, the structural phases determined here should not be regarded as those defined in the thermodynamic limit, due to the finite size effect. The pseudo is omitted in the following.

[38] S. Neidle, *Principles of Nucleic Acid Structure* (Elsevier, Amsterdam, 2008).

[39] V. Berl, I. Huc, R. G. Khoury, M. J. Krische, and J.-M. Lehn, Nature (London) **407**, 720 (2000).

[40] H. Goto, H. Katagiri, Y. Furusho, and E. Yashima, J. Am. Chem. Soc. **128**, 7176 (2006).

[41] R. R. Hudgins and M. F. Jarrold, J. Am. Chem. Soc. **121**, 3494 (1999).

[42] D. T. Kaleta and M. F. Jarrold, J. Am. Chem. Soc. **125**, 7186 (2003).